Spectroscopy of Molecular Junction Networks Obtained by Place Exchange in 2D Nanoparticle Arrays

ARTICLE *in* THE JOURNAL OF PHYSICAL CHEMISTRY C · DECEMBER 2007

Impact Factor: 4.77 · DOI: 10.1021/jp077095c

6 AUTHORS, INCLUDING:

Laetitia Bernard
Empa - Swiss Federal Laboratories for Materi…
18 PUBLICATIONS **406** CITATIONS
SEE PROFILE

Michel Calame
University of Basel
72 PUBLICATIONS **2,442** CITATIONS
SEE PROFILE

Jianhui Liao
Peking University
32 PUBLICATIONS **701** CITATIONS
SEE PROFILE

THE JOURNAL OF PHYSICAL CHEMISTRY C LETTERS

2007, *111,* 18445−18450
Published on Web 11/22/2007

Spectroscopy of Molecular Junction Networks Obtained by Place Exchange in 2D Nanoparticle Arrays

Laetitia Bernard,[†,‡] Yavor Kamdzhilov,[§] Michel Calame,*[,†] Sense Jan van der Molen,[†,#] Jianhui Liao,[†] and Christian Schönenberger[†]

Department of Physics, University of Basel, 4056 Basel, Switzerland, and Department of Chemistry, University of Basel, 4056 Basel, Switzerland

Received: September 4, 2007; In Final Form: November 6, 2007

Well ordered nanoparticle arrays were prepared on Si/SiO_2 surfaces from alkanethiol-coated Au nanoparticles via self-assembly and micro-contact printing. We study the insertion of conjugated molecular species within the nanoparticle arrays via spectroscopic and electrical transport measurements. Upon exchange of the alkanethiol chains with the conjugated oligomers, the conductance of the network increases by one to 3 orders of magnitude. In addition, the absorption spectra in the visible light range show a red-shift of the surface plasmon resonance (SPR). The latter shift, which is due to the difference in permittivity between alkanes and conjugated oligomers, can be understood within Mie and Maxwell−Garnett theory. Finally, infrared absorption spectra provide direct spectroscopic evidence that the conjugated oligomers can be not only inserted but also, subsequently, fully removed from the nanoparticle arrays via place-exchange. The reversibility of the exchange process demonstrates the potential of these structures as a platform for molecular electronics.

Introduction

Molecular electronics is attracting an increasing research attention, mainly supported by the possibilities of tailoring molecules to achieve specific electronic functions.[1] For that reason, the development of robust experimental platforms where molecular junctions can be tested systematically and at large scale is of great importance to this field of research. Metallic nanoparticles in the nanometer scale can be easily synthesized and assembled to provide a versatile scaffold, suitable for a variety of applications.[2] We have recently demonstrated the insertion of conjugated molecules in two-dimensional arrays of alkanethiol-capped gold nanoparticles by molecular exchange.[3] Transport measurements showed a change in the electrical conductance by 1−3 orders of magnitude and suggested that the process is reversible. Such structures therefore represent an interesting and stable test-bed for systematically characterizing a variety of molecular junctions in a flexible and upscaleable device approach.

We present here an in-depth analysis of the molecular exchange based on electrical transport measurements, ultraviolet−visible (UV−vis) spectroscopy and infrared (IR) spectroscopy. All three complementary approaches demonstrate that conjugated molecules can indeed be inserted within nanoparticle arrays, leading to well-defined molecular devices. Moreover, the spectroscopic data permit us to quantify the efficiency of the molecular exchange. Finally, we demonstrate that the inserted molecules can be fully removed by subsequent exchange steps.

Experimental Methods

Nanoparticle Synthesis and Functionalization. Charge stabilized Au nanoparticles were synthesized by the reduction of chloroauric acid in water.[4] To obtain a 100 mL aqueous solution of Au nanoparticles, a solution with 1 mL of $HAuCl_4 \cdot 4H_2O$ (1%) in 79 mL of H_2O was first prepared. A 20 mL reducing solution with 4 mL of trisodium acid (1%) and 80 μL of tannic acid (1%) in 16 mL of H_2O was then added rapidly to the Au solution (all solutions at 60 °C). The mixed solution was boiled for 10 min before being cooled down to room temperature. A continuous stirring was applied throughout the process. The resulting reddish solution contained typically 10 nm neutral Au nanoparticles at a concentration of $\sim 10^{13}$/mL. A statistics over ~14 000 particles gives an average diameter of 9.2 nm with a 0.7 nm standard deviation. The diameter of the nanoparticles can be adjusted between 5 nm and 20 nm by tuning the tannic acid concentration. Unless otherwise stated, all reagents were purchased from Fluka and used as received. For all reactions, deionized water was used.

The encapsulation of the nanoparticles in an alkanethiol monolayer was performed following the procedure developed by Huang *et al.*[5] A first centrifugation (typically: 10 mL solution at 13 000 rpm for 45 min) step permits the transfer of the particles from water to ethanol. After a brief ultrasonic treatment, the nanoparticle solution was mixed with 4 mL of a 0.1 M alkanethiol solution in ethanol. The reaction was carried out

* To whom correspondence should be addressed. Address: Department of Physics, University of Basel, Klingelbergstrasse 82, CH-4056 Basel, Switzerland. E-mail: michel.calame@unibas.ch. Tel.: +41 61 267 3697. Fax: +41 61 267 3784.
[†] Department of Physics, University of Basel, 4056 Basel, Switzerland.
[‡] Present address: Department of Electrical Engineering, Yale University, CT-06520-8284 New Haven, CT, USA.
[§] Department of Chemistry, University of Basel, 4056 Basel, Switzerland.
[#] Present address: Kamerlingh Onnes Laboratorium, Universiteit Leiden, Niels Bohrweg 2, 2333 CA Leiden, The Netherlands.

10.1021/jp077095c CCC: $37.00

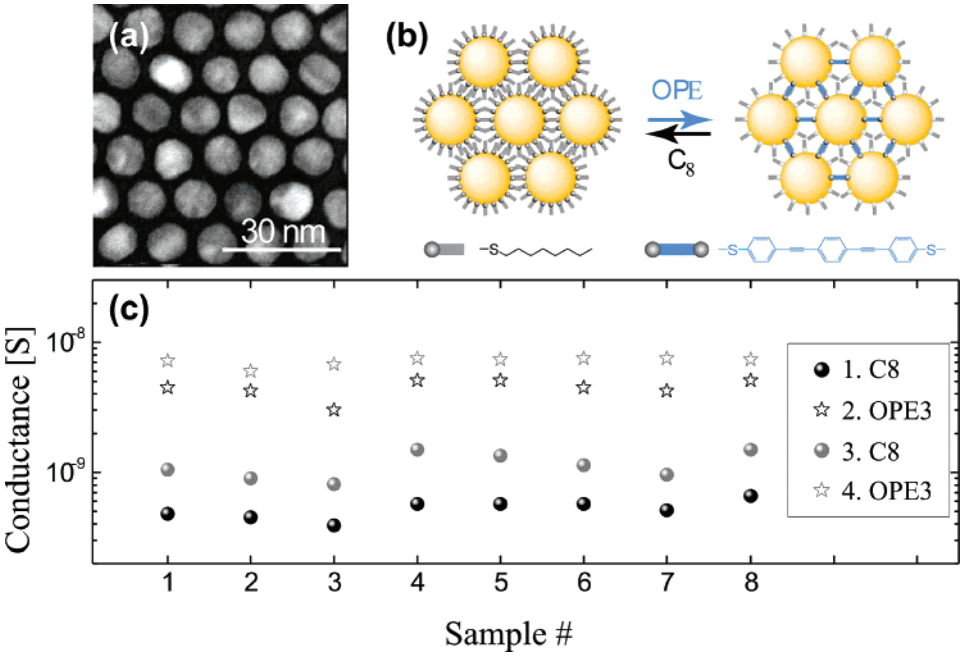

Figure 1. (a) TEM image of a micro-contact printed self-assembled nanoparticle array. (b) Schematic of the molecular exchange from C8 to OPE3 and back. (c) Electrical conductance for eight arrays during the successive steps of a molecular exchange.

typically for 24 h. The precipitate consisting of the capped nanoparticles is then washed with ethanol to discard excess alkanethiols. The capped nanoparticles were finally suspended in chloroform via an ultrasonic treatment.

Arrays Fabrication. Au nanoparticle arrays were obtained by self-assembly at an air−water interface.[6] In this process, the interparticle distance is controlled by the length of the capping alkane layer. Typically, we added 400 μL of nanoparticles in chloroform to a Teflon container filled with pure water. After allowing the solvent to evaporate for a few minutes (fume hood), a self-assembled monolayer (2D array) of particles was formed. The process can easily be followed by naked-eye, watching how the ruby-red nanoparticle solution changes color during assembly to finally yield a golden, metallic-looking nanoparticle film.

The self-assembled structures were transferred onto Si/SiO_2 (for transport measurements) or CaF_2 (for optical characterization) substrates via polydimethysiloxane (PDMS) stamps. The stamps were prepared by mixing a prepolymer gel with its curing agent (Sylgard 184, Corning) on a master structure with the desired pattern. The master was fabricated by UV lithography in a negative resist (ma-N 400, micro resist technology). The polymer mix was degassed for 30 min at room temperature and cured at 60 °C for 1.5 h. Once baked, the PDMS layer could be peeled off from the master and cut into the required shape.

The stamping procedure yields uniform 2-D monolayers of long-range hexagonally packed nanoparticles (typical grain size in the μm^2 range), spaced by interdigitated alkane chains (see Figure 1a). The long-range order achieved with this relatively straightforward method allows the fabrication of compact arrays over large areas (mm^2), particularly suitable for spectroscopic measurements.

Molecular Exchange. The procedure, schematically depicted in Figure 1b, consisted in immersing the stamped array in 2 mL of a 1 mM solution of dithiolated oligo(phenylenethynylene) (OPE3) in THF at room temperature. The solution was bubbled with Ar before immersion, and the arrays were kept in solution during 24 h under an Ar atmosphere. After this period, we observed a saturation of the resistance for electrically contacted arrays.[3] For experiments where multiple exchange steps were performed, the back-exchange to octanethiol (C8) followed a similar protocol.

Results and Discussion

Transport Measurements. The electrical properties of the arrays were studied for printed lines of nanoparticles about 10 μm in width. Au contact pads, with a typical spacing of 10 μm, were deposited on top of the arrays by electron-beam evaporation using a transmission electron microscopy (TEM) grid as shadow mask. The conductance of the arrays was measured in a prober stage via an IV-converter. The maximum bias voltage applied was 10V. Figure 1c shows conductance data for eight 10×10 μm^2 arrays acquired during an exchange process following the sequence C8 (1) → OPE3 (2) → C8 (3) → OPE3 (4). As previously observed,[3] a first exchange to OPE3 (1 → 2) increases the conductance of the arrays, by about an order of magnitude. As expected, a back-exchange to C8 (2 → 3) decreases the conductance of the arrays, however to a slightly larger value than the initial conductance. We emphasize here that the exchange is performed in a 2D array structure, which is a quite confined geometry. The initial alkanethiol coating of the nanoparticles was performed in solution, a more favorable situation to achieve high-density coverage. We therefore anticipate a slightly sparser (and hence less insulating) alkane coverage of the nanoparticles after back-exchange. We will come back to this point when discussing the optical absorption data, later in the text. A final exchange to OPE3 (3 → 4) increases again the conductance of the array, although to a slightly larger final value than the first exchange did. Building on the previous argument, we can expect that the insertion of the OPE3 compounds will now be facilitated, as compared to the first exchange to OPE3 (1 → 2). We therefore expect an improved inter-linking of neighboring nanoparticles, leading to a slightly larger conductance of the array. The conductance variation from sample to sample at each exchange step can be attributed to local variations in the geometry of the nanoparticles arrangement. Note that these differences are preserved throughout the exchange, which indicates a good mechanical stability of the arrays.

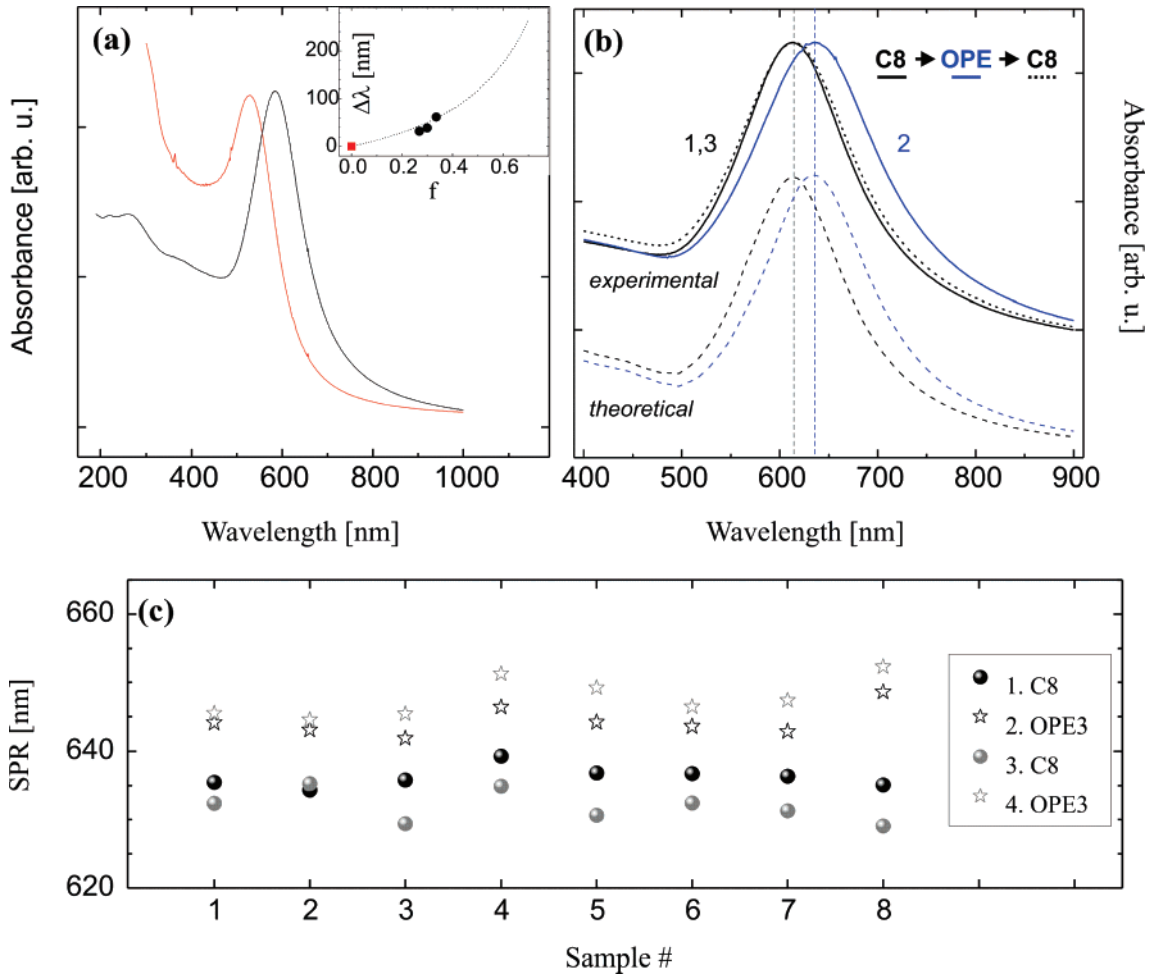

Figure 2. (a) UV−vis absorption spectra for hexadecanethiol (C16)-capped nanoparticles in chloroform (left curve, red) and as an array (black), showing the red-shift upon array formation. The inset shows the red-shift $\Delta\lambda$ as a function of filling factor f for arrays with different alkanethiol spacers (black solid circles; left to right: C_{16},C_{12},C_8), compared to the value in solution (red square). The dotted line is the red shift calculated from the Maxwell−Garnett approach, i.e.: eqs 1 and 5. (b) Visible absorption spectra (top) of a C8 array for a three-steps exchange: before (black), after OPE3 exchange (blue), after back-exchange (dotted black). Fits according to Mie and Maxwell−Garnett theory (dashed curves, *y*-shifted for clarity) yield $\Delta\epsilon = 0.5$. (c) Surface plasmon resonance peak position at the successive steps of molecular exchange. The absorption data were taken on the same eight arrays as the transport data shown in Figure 1c.

Surface Plasmon Resonance. We also assess the exchange process by monitoring the optical absorption of nanoparticle arrays close to the surface plasmon resonance (SPR) of the colloids. In a diluted solution, 10 nm alkanethiol-coated gold nanoparticles typically have their SPR around 530 nm, as shown in Figure 2a (left, red curve). For stamped arrays (typically 8 × 8 mm^2 arrays), the SPR exhibits a substantial red shift due to the interaction between neighboring nanoparticles (Figure 2a, black curve). To describe both the resonance and the red shift due to arrays formation, we turn to Mie theory and Maxwell−Garnett theory.[7]

The optical absorption cross-section σ of nanoparticles can be calculated via Mie theory. For our devices, we can use the quasi-static approximation because the cluster size (radius $R \approx$ 5 nm) is much smaller than the interacting wavelength. In this case, the fields inside the cluster are considered constant and we can use a simplified expression for the absorption cross-section[8] (dipolar approximation, first order):

$$\sigma = 12\pi \frac{\omega}{c}{\epsilon_m}^{3/2}R^3 \frac{\epsilon_2(\omega)}{[\epsilon_1(\omega) + 2\epsilon_m]^2 + {\epsilon_2}^2(\omega)} \qquad (1)$$

where ϵ_m is the permittivity of the surrounding medium (real) and $\epsilon(\omega) = \epsilon_1(\omega) + i\epsilon_2(\omega)$ is the permittivity of the cluster (complex). The latter is derived for bulk metal using a Drude−Lorentz−Sommerfeld model:

$$\epsilon_1(\omega,R) = 1 - \frac{{\omega_p}^2}{\omega^2 + \Gamma^2(R)} + \epsilon_{1,\mathrm{core}}$$

$$\epsilon_2(\omega,R) = \frac{{\omega_p}^2\Gamma(R)}{\omega(\omega^2 + \Gamma^2(R))} + \epsilon_{2,\mathrm{core}} \qquad (2)$$

where Γ is a phenomenological damping constant related to the mean free path of electrons; ω_p is the plasmon frequency, and ϵ_{core} is the core electrons' contribution (real and imaginary parts) to the permittivity. The latter contribution was extracted from reference experimental optical constants for bulk gold.[9] For small clusters, the damping is strongly affected by the size of the object, as collisions with the cluster boundaries become dominant. Hence, the damping constant Γ explicitly depends on R:

$$\Gamma(R) = \frac{\upsilon_F}{l_\infty} + A\frac{\upsilon_F}{R} \qquad (3)$$

where υ_F is the Fermi velocity and A denotes a proportionality factor of order unity.[10] Equations 1−3 give a good description

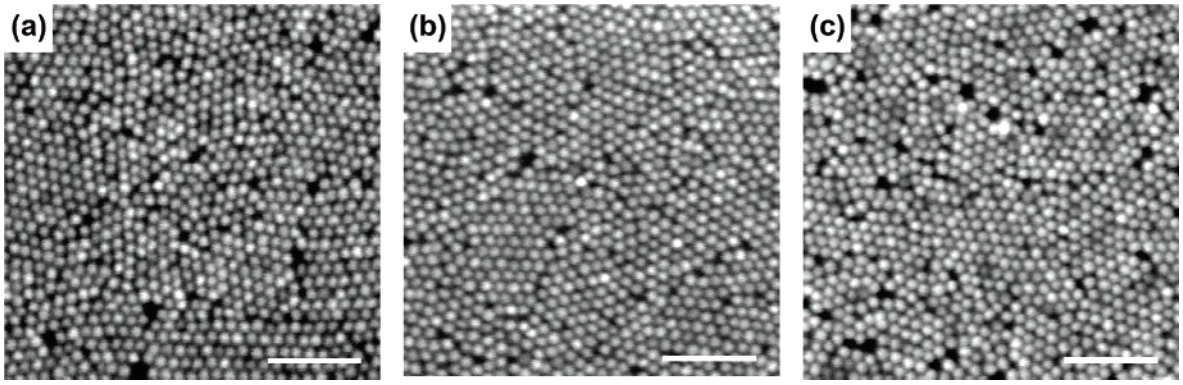

Figure 3. SEM images of a nanoparticle array at various stages of a molecular exchange: (a) C8-capped nanoparticle arrays as-prepared; (b) after exchange with OPE3; (c) after back-exchange to C8. The structure of the array is preserved during exchange. Scale bar: 100 nm for all images.

of the extinction of light in metallic clusters of diameters ~10 nm, relevant for our case. This model holds as long as there is no interaction between the clusters (diluted system) and the total extinction is the sum of each cluster's contribution. In the more confined array arrangement, the nanoparticles interact with each other and the resonance of the surface plasmon is shifted to longer wavelengths (red shift). This interaction can be accounted for by replacing the permittivity of the system by an *effective medium* permittivity ϵ_{eff}. The latter contribution depends on the average volume fraction of particles, described by the filling factor $f = V_{\text{clusters}}/V_{\text{total}}$. The Maxwell−Garnett effective medium theory[11,12] gives

$$\epsilon_{\text{eff}}(\omega) = \epsilon_{\text{m}}\frac{1 + 2f\Lambda}{1 - f\Lambda} \qquad \Lambda = \frac{\epsilon(\omega) - \epsilon_{\text{m}}}{\epsilon(\omega) + 2\epsilon_{\text{m}}} \tag{4}$$

and the condition for resonance corresponds to

$$\epsilon_1(\omega_{\text{sp}})(1 - f) + \epsilon_{\text{m}}(2 + f) = 0 \tag{5}$$

where ω_{sp} is the frequency for which the surface plasmon absorption is maximum. From eq 5, it is qualitatively clear that ω_{sp} depends on the filling factor f, as indeed observed in Figure 2a. Note that in solution, we can take $f = 0$, giving the usual Mie resonance condition: $\epsilon_1 + 2\epsilon_{\text{m}} = 0$.

The model described by eqs 1−5 is appropriate for nanoparticles isotropically distributed and separated by a homogeneous matrix and at low filling factors. Interference effects and reflection losses can additionally contribute to the optical absorption in thin films, in particular for multilayer films.[13] The MG effective medium theory however provides in many cases a sufficient description and has been successfully applied to describe the absorption properties of Au and Ag nanoparticle thin films in different matrices,[14] including at filling factors up to $f = 0.5$.[14c]

We first apply the MG theory for networks consisting of nanoparticles covered with C8 (octanemonothiol), C12 (dodecanemonothiol), or C16 (hexadecanemonothiol) thiolated alkanes. From transmission electron microscopy measurements (TEM), we estimated inter-particle distances of $d_{\text{C8}} = 2.6$, $d_{\text{C12}} = 2.8$, and $d_{\text{C16}} = 3.0 \pm 0.02$ nm in such networks, respectively. By using longer alkanethiol spacers, we can create arrays with larger interparticle distances and lower f. From the interparticle distances, we infer a filling factor f for all three types of devices, i.e., $f_{\text{C8}} = 0.34$, $f_{\text{C12}} = 0.30$, and $f_{\text{C16}} = 0.27$.[15] The inset in Figure 2a displays the red shift of the SPR peak, $\Delta\lambda$, measured for the three types of arrays and plotted as a function of filling factor f. Closer nanoparticles, correspondingly, larger filling factors, will result in a larger red shift. Via MG theory, we can calculate the theoretical red-shift as a function of f (inset Figure 2a, dotted line). Note that in our calculation we use $\epsilon_{\text{m}} = 2.5$, which will appear justified from the fits shown in Figure 2b. We observe a reasonable agreement between theory and data, justifying the use of combined Mie and Maxwell−Garnett theories for our networks.

We can now consider C8 networks in which oligo(phenylthynylene) compounds (OPE3) have been inserted via a place-exchange reaction. The position of the SPR peak was investigated at three stages of molecular exchange between C8 and OPE3 molecules (see Figure 2b, top curves): (1) C8-as-prepared (black); (2) after OPE3-exchange (blue); (3) after C8-back-exchange (dotted gray). We observe in this case a red shift of about 20 nm between (1) and (2). An average over five samples gives a typical shift of 15 ± 5 nm. We further observe that no substantial modification in the arrangement of the particles was noticeable in SEM images before and after exchange (Figure 3). The observed red shift after OPE3-exchange can therefore be attributed to the sole effect of the surrounding medium change. As previously indicated by transport measurements, these data further support the reversibility of the exchange process. The dashed curves in Figure 2b (bottom) are fits to the absorption spectra based on the dipolar approximation derived from Mie theory and Maxwell−Garnett theory. We used two fitting parameters, namely the proportionality factor A and the permittivity of the surrounding medium ϵ_{m}. We find good correspondence between the experimental curves and fits for $A = 2.0 \pm 0.2$[16] and $\epsilon_{\text{m}} = 2.5 \pm 0.1$ before exchange (the value used in Figure 2a) and $\epsilon_{\text{m}} = 3.0 \pm 0.1$ after exchange. Reported permittivity values for alkanes typically range between $\epsilon_{\text{alk}} = 1.9-2.2$.[17,18] Our value of 2.5 is slightly larger than expected, which might be due to the influence of the nearby CaF_2 substrate ($\epsilon_{CaF_2} = 6.8$). Values for OPE3 and related conjugated oligomers are expected to be larger, $\epsilon_{\text{OPE}} = 3.1-3.9$.[19,20] The shift observed of $\Delta\epsilon = 0.5$ is substantially smaller than anticipated from the literature values, indicating that exchange is not 100%, but rather partial. We therefore estimate that, after molecular exchange, only 20−40% of the surface area of the nanoparticles is occupied by OPE molecules. Murray *et al.*[21] showed that exchanging distinct alkane species on nanoparticles in solution does not lead to the full removal of all of the initial species. We expect this to be even more the case here, given that stamped 2D nanoparticle arrays form a more confined geometry than free floating nanoparticles.

In Figure 2c, we report the peak position of the SPR resonance for the same eight arrays as in Figure 1c, during an exchange following the sequence C8 → OPE3 → C8 → OPE3. The optical

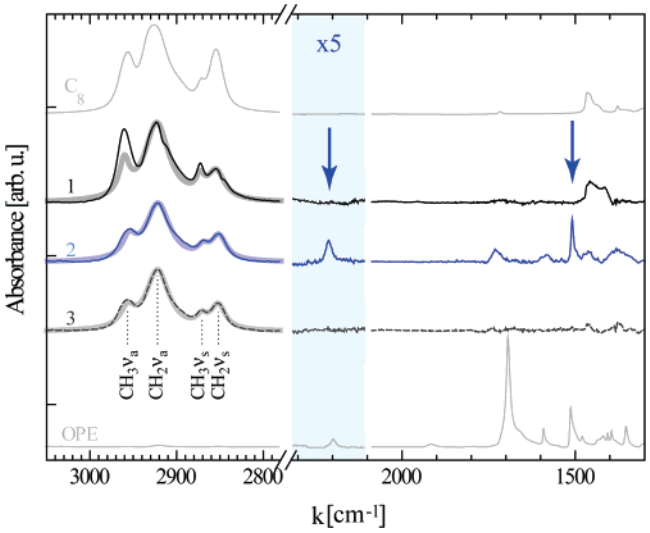

Figure 4. FTIR spectra, from top to bottom: pure C8 (liquid), as-prepared C8-array (1), same array after OPE3-exchange (2), same array after C8 back-exchange (3), OPE3 imbedded in a KBr matrix (solid). The thicker gray traces on the left side of spectra 1−3 are Lorentzian multi-peak fits. The blue arrows point to specific signatures of the OPE3 compound.

absorption data correlate well with the transport data of Figure 1c, showing, as expected, a red-shifted absorption peak for arrays with larger conductance. Note the absorption data were taken here on arrays covering a small area (typically $\leq 10 \times 10$ μm^2, located between the contact pads) and those of Figure 2b were measured for nanoparticle arrays covering a few mm^2. The shifts observed for the small arrays are within the range of the observed shifts for larger arrays ($\Delta\lambda = 15 \pm 5$ nm). From the transport measurements, we anticipated a lower alkanethiol density at step 3 than at step 1 (see above). As a consequence, we expect a slight blue-shift (lowering of the dielectric constant) between step 1 and step 3, because a smaller fraction of the interparticle space will be occupied by alkanethiols and be in ambient ($\epsilon_{air} \approx 1$) at step 3. This is indeed what we observe in most cases, supporting the initial assumption of lower alkanethiol density at step 3. We therefore also await a facilitated insertion of the conjugated compound during the second OPE3 exchange (3 → 4), as argued previously. As seen on the data, the second red shift is slightly larger than the first one (1 → 2), confirming a larger dielectric constant for the inter-particle medium at step 4 than at step 2. In brief, the SPR data can not only be well understood within the Mie and Maxwell−Garnett theories but also are in good agreement with transport measurements.

IR Spectroscopy. Further insight into the exchange process and the molecular composition of the arrays can be inferred from Fourier-transform infrared spectroscopy (FTIR). Figure 4 displays a series of spectra corresponding to the three stages of the exchange between C8 and OPE3 as described above. Spectra for pure C8 (top) and OPE3 (bottom) are also shown in gray. Spectral comparisons with reported experimental data[22] and density-functional theory (DFT) calculations[23] have been performed to assign the most relevant peaks. The optical response of the C8-as-prepared array (1) exhibits the typical features of alkane chains, i.e., the methylene (CH_2) and methyl (CH_3) stretching vibrations around 3000 cm^{-1} and deformation around 1450 cm^{-1}. The symmetric (ν_s) and antisymmetric (ν_a) stretching modes around 3000 cm^{-1} are emphasized in Figure 4. The thicker, gray curves in spectra 1−3 are Lorentzian multiple-peak fits, using the spectrum of pure C8 as reference (the relative amplitudes of the absorption peaks were kept identical). In spectrum 1 (initial state), the proportion of CH_3 versus CH_2 is larger than expected for pure C8. We attribute this effect to remaining traces of ethanol present in the nanoparticle functionalization procedure. This effect is also visible in the 1450 cm^{-1} region (OH and COH bending vibrations). Note that the CH_3/CH_2 ratio, as estimated from the ratio of the surface area below the respective fitted Lorentzian peaks, is in accordance with that of pure octanethiol (1/7) for the two subsequent spectra (2 and 3) and the feature in the 1450 cm^{-1} region is strongly reduced. This suggests that the ethanol traces are removed during the exchange.

Spectrum 2, obtained after OPE3-exchange, unambiguously reveals the coexistence of C8 and OPE3 molecules. Indeed, whereas one can still identify C8 stretching features, the C≡C at ∼2200 cm^{-1} (zoomed 5× for clarity), and C−C at 1500 cm^{-1} ring vibrations of the OPE3 molecules appear clearly (arrows). This observation proves the insertion of OPE3 within the array. That the C8 vibrations are still strongly present after exchange confirms the partial character of molecular exchange, in agreement with the SPR measurements. We note the absence of the intense C═O vibration from the acetyl protection groups at ∼1700 cm^{-1}, clearly present in the free OPE3 spectrum. This confirms that the OPE3 are well deprotected and provide thiol functionalities for chemical attachment at the surface of the gold nanoparticles. Finally, after back-exchange of the array (spectrum 3), the OPE3 signature is no longer observed, indicating that OPE3 can be inserted and fully removed. The relative amplitudes of the signal for the alkanethiol vibrations increases only slightly to reach 71% of that in spectrum 1. As anticipated before, from both the transport measurements and the SPR data, this further supports the view that the density of C8 molecules decreases between the "virgin" case 1 and case 3 after back-exchange. From the Lorentzian fits to the alkanethiols peaks, we obtain a relative change in intensity between spectra 1 and 2 ranging from 20% to 30% (ratio of the surfaces below the peaks). This represents an estimate for the exchange efficiency which is well within the range obtained from the UV−vis measurements. We further stress here that a large fraction of molecules on the particles are C8 alkanethiols in all stages of the exchange. We think that this fact is crucial for the stability of the array. The alkanethiols provide a sufficient interdigitation to preserve the structural integrity of the array at all times, as we did not observe any degradation after up to 7 successive exchange steps.

Conclusion

In summary, we combined visible and IR spectroscopies with transport measurements to characterize a place-exchange process within nanoparticle arrays. We find that OPE3 molecules partially replace the alkanethiols capping the nanoparticles upon exchange. Remarkably, the exchange is found to be reversible with no signature of the OPE3 molecules after a back-exchange procedure, in good agreement with transport measurements. We find that Mie and Maxwell−Garnett theories provide an adequate description for the arrays absorption in the visible and infer dielectric constants for the molecular matrix in agreement with commonly admitted values. Further support for the exchange is provided by the clear fingerprint of the OPE3 compound visible in the IR spectra.

The characterization of molecular exchange by these three independent techniques provides a better understanding of the exchange process, an essential feat in the perspective of molecular electronics. Additional studies are currently underway

that address the kinetics and mechanics underlying the exchange process. As such, the easy insertion and removal of molecules in nanoparticle systems already ascertain the potential of network structures as a flexible and upscaleable platform for molecular electronics.

Acknowledgment. We acknowledge M. Langer and A. Pfaltz for synthesizing the OPE3 molecules and J. Wirz for providing access to his spectroscopy equipment. S.J.v.d.M. acknowledges The Netherlands Organization for Scientific Research, NWO ("Talent stipendium"). This work was supported by the Swiss National Center of Competence in Research "Nanoscale Science" (NCCR), the Swiss National Science Foundation (SNF), and the European Science Foundation EUROCORES program on Self-Organized Nanostructures (SONS).

References and Notes

(1) (a) Nitzan, A.; Ratner, M. *Science* **2003**, *300*, 1384. (b) Tao, N. *Nature Nanotechnology* **2006**, *1*, 173. (c) Selzer, Y.; Allara, D. L. *Annu. Rev. Phys. Chem.* **2006**, *57*, 593.

(2) For reviews, see, e.g.: (a) Shipway, A. N.; Katz, E.; Willner, I. *Chem Phys Chem* **2000**, *1*, 18. (b) McConnell, W. P.; Novak, J. P.; Brousseau, L. C.; Fuierer, R. R.; Tenent, R. C.; Feldheim, D. L. *J. Phys Chem. B* **2000**, *104*, 8925.

(3) Liao, J.; Bernard, L.; Langer, M.; Schönenberger, C.; Calame, M. *Adv. Mater.* **2006**, *18*, 2444.

(4) (a) Slot, J.; Gueuze, H. *Eur. J. Cell. Biol.* **1985**, *38*, 87. (b) Brust, M.; Walker, M.; Bethell, D.; Schiffrin, D.; Whyman, R. *J. Chem. Soc., Chem. Commun.* **1994**, 801.

(5) Huang, S.; Tsutsui, G.; Sakaue, H.; Shingubara, S.; Takahagi, T. *J. Vac. Sci. Technol. B* **2001**, *19*, 115.

(6) Santhanam, V.; Andres, R. P. *Nano Lett.* **2004**, *4*, 41.

(7) For a general reference, see, e.g.: Kreibig, U.; Vollmer, M. *Optical properties of metal clusters*; Springer-Verlag: Berlin, 1995.

(8) Mie, G. *Ann. Phys.* **1908**, *25*, 377.

(9) Lide, D. R. ed., *Handbook of Chemistry and Physics*, 85th ed.; CRC Press: Boca Raton, FL, 2004−2005.

(10) Kreibig, U.; Genzel, L. *Surf. Sci.* **1985**, *156*, 678.

(11) Garnett, J. M. *Philos. Trans. R. Soc. London* **1904**, *203*, 385.

(12) (a) Cohen, R. W.; Cody, G. D.; Coutts, M. D.; Abeles, B. *Phys. Rev. B* **1973**, *8*, 3689. (b) Dalascu, D.; Martinu, L. *J. Appl. Phys.* **2000**, *87*, 228.

(13) Ung, T.; Liz-Marzan, L. M.; Mulvaney, P. *Colloids Surf.* **2002**, *202*, 119.

(14) (a) Wang, J.; Lau, W. M.; Li, Q. *J. Appl. Phys.* **2005**, *97*, 114303. (b) Mandal, S. K.; Roy, R. K.; Pal, A. K. *J. Phys. D* **2002**, *35*, 2198. (c) Sawitowski, T.; Miquel, Y.; Heilmann, A.; Schmid, G. *Adv. Funct. Mater.* **2001**, *11*, 435.

(15) The filling factor f was calculated for a unit cell (containing one cluster) with base $0.74\cdot(Ø + d_{Cn})^2$ and height $(Ø + 2l_m)$; d_{Cn} is the interparticle distance as estimated from TEM measurements, and l_m is the alkanethiol length.

(16) The parameter A has been shown to depend on the material, geometry, packing and immediate surrounding of the nanaoparticles and can substantially differ from unity. See, e.g., ref 10 and: Quiten, M. *Z. Phys. B* **1996**, *101*, 211 and references therein.

(17) Israelachvili, J. *Intermolecular and Surface Forces*; Academic Press: New York, 1985.

(18) (a) Porter, M.; Bright, T.; Allara, D.; Chidsey, C. *J. Am. Chem Soc.* **1987**, *109*, 3559. (b) Rampi, M.; Schueller, O.; Whitesides, G. *Appl. Phys. Lett.* **1998**, *72*, 1781.

(19) (a) Granqvist, C.; Hunderi, O. *Phys. Rev. B* **1977**, *16*, 3513. Mulvaney, P. *Langmuir* **1996**, *12*, 788. (b) Schmitt, J.; Mächtle, P.; Eck, D.; Möhwald, H.; Helm, C. *Langmuir* **1999**, *15*, 3256.

(20) (a) Stapleton, J.; Harder, P.; Daniel, T.; Reinard, M.; Yao, Y.; Price, D.; Tour, J.; Allara, D. *Langmuir* **2003**, 8245. (b) Tammer, M.; Monkman, A. P. *Adv. Mat.* **2004**, *14*, 210.

(21) Hostetler, M.; Templeton, A.; Murray, R. *Langmuir* **1999**, *15*, 3782.

(22) (a) Bellamy, L. J. *The Infra-red Spectra of Complex Molecules*; Wiley: New York, 1975. (b) Günzler, H.; Gremlich, H. *IR spectroscopy;* Wiley-VCH, 2002.

(23) DFT calculations were performed using the Gaussian 03 software package: Frisch, M.; *et al*. *Gaussian 03*; Gaussian Inc.: Wallingford, CT, 2004.